ORIGINAL PAPER

Surface Settlement Induced by Subway Tunnel Construction Based on Modified Peck Formula

Qianjin Zhang · Ke Wu · Shuaishuai Cui · Yalin Yu · Zheng Zhang · Jiahui Zhao

Abstract A surface subsidence model is established to address the issue of the increase in surface settlement with time. Considering the effects of time factors and depth on surface subsidence, the formula was derived and it was used to calculate the three-dimensional space–time prediction of two-line tunnel settlements in construction processes. Thus, we obtain the calculation method of ground settlement for single- and double-line tunnels. Research relies on Shenzhen Metro Line 7 project. On the basis of the comparison between FLAC 3D calculation software and on-site monitoring, the reliability of the proposed modified Peck formula for the calculation of surface settlement induced by shallow tunnel construction is verified. Research indicates that (1) the proposed calculation method for ground settlement induced by subway tunnel construction is accurate; (2) the modified Peck formula predicts soil settlement at different times and depths; and (3) the revealed surface settlement law is consistent with numerical simulation and measured results, which can effectively reveal the mechanism and law of surface settlement caused by tunnel excavation.

1 Introduction

With rapid economic development and continuous expansion of urban space, underground traffic engineering has been adopted by an increasing number of cities due to its ability to effectively use underground space and relieve traffic. Tunnel excavation in underground traffic engineering will cause settlement of soil within a certain range above the tunnel and change the original equilibrium state of the soil. The planned routes of the metro are often located in densely populated urban areas with numerous buildings. When the settlement of the soil reaches a certain level, it may have a destructive effect on the safety of surface buildings. Therefore, predicting ground settlement in subway construction is an important research topic.

At present, many studies on ground settlement in subway construction are available. Peck believes that the surface will form a settling trough during tunnel excavation. Assuming that the soil is undrained, the volume of the settling trough should be equal to the loss volume of the soil, and the shape of the surface lateral settling trough above the tunnel is similar to a normal distribution curve (Peck 1969). Litwiniszyn believes that tunnel excavation is assumed to be a plane strain problem, and excavating the tunnel soil is

Q. Zhang · K. Wu (✉) · S. Cui · Y. Yu ·
Z. Zhang · J. Zhao
School of Civil Engineering, Shandong University, Jinan,
China
e-mail: wuke@sdu.edu.cn

regarded as the sum of the excavation of numerous micro-units. After such treatment, the influence of excavation on the ground can also be regarded as the superposition of the influence on each unit body (Litwiniszyn 1956). Li Xinzhi obtained the value and distribution characteristics of surface settlement through a geomechanical model test and analyzed the influence of construction measures on the settlement law (Li et al. 2012; An 2015; Chen et al. 2014). Yang Yandong used ANSYS to simulate shield tunnel construction and obtain surface subsidence patterns (Yandong et al. 2014). Scholars have conducted several studies on surface settlement (Gang and Yangkan 2016; Zhang et al. 2016). However, few studies have been conducted on the combination of theoretical analysis, actual monitoring, and numerical simulation, and the influence of time factors on surface settlement.

To solve the existing problems, this paper, which is based on the Peck formula and Pearl curve and considers time factors, derived the formula for the prediction of surface settlement during tunnel construction. Relying on construction cases, this paper verified the correctness of the formula through numerical simulation and monitoring data to obtain the surface settlement patterns.

2 Application of Peck Formula in Predicting Surface Settlement

Tunnel excavation must break the original mechanical balance and cause stress redistribution, thereby causing surrounding rocks to move toward the excavation area. Peck gathered numerous on-the-spot measurement experiences and suggested that the shape of the settling trough that forms on the surface after tunnel excavation is similar to the normal distribution. Peck believes that the formation of the settling trough is mainly caused by ground loss (Ke et al. 2016; Zhu et al. 2012; Changming et al. 2018; Kang et al. 2014). Assuming that the soil is undrained and its volume is incompressible, the point where the sedimentation trough has the largest value should be located at the midline of the tunnel. Figure 1 illustrates the shape of the surface settling trough. Equations 1 and 2 express the formula for surface settlement:
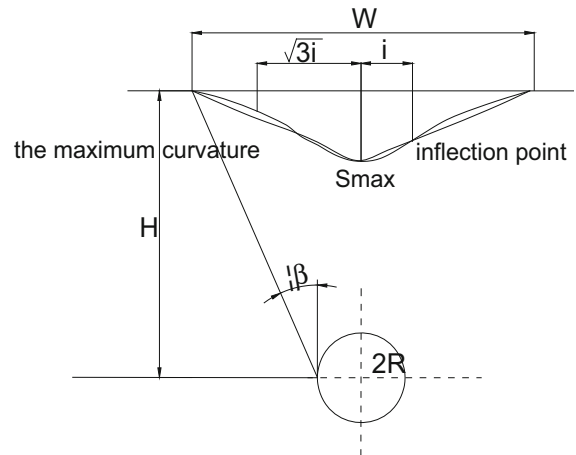
Fig. 1 Surface settling trough

$$S_{(x)} = S_{max} \cdot \exp\left(-\frac{x^2}{2i^2}\right) \tag{1}$$

$$S_{max} = \frac{V_{loss}}{i\sqrt{2\pi}} \tag{2}$$

where $S_{(x)}$ is the amount of surface settlement, x is the horizontal coordinate of the ground with the center of the tunnel as the origin, V_{loss} is the soil loss rate of the unit length of the tunnel, i is the width coefficient of the surface settlement trough, and η is the soil loss rate. The values of V_{loss} and i are closely related to the final prediction.

Peck's i and V_{loss} formulas are as follows:

$$V_{loss} = \pi R^2 \tag{3}$$

$$i = R\left(\frac{H}{2R}\right)^2 \tag{4}$$

where R is the radius of the tunnel, and H is the depth of the tunnel's axis from the ground.

3 Theoretical Analysis Based on the Modified Peck Formula

Tunnel excavation is a dynamic process. During construction, the settlement of the measuring point increases with the change in tunneling time. Therefore, the prediction of settlement combined with time and space factors can be increasingly accurate.

3.1 Pearl Curve Model

To study the time–space process of surface settlement, a reasonable space–time model for ground settlement needs to be established first. The nature of the Pearl curve is similar to that of tunnel excavation. The early development is slow, and then it enters a stage of high-speed development. The late-stage change speed is slow. This development trend is in line with the theory of current mainstream tunnel vertical settlement.

The Pearl curve is a typical three-stage S-curve, as shown in Fig. 2. The deformation formula is as follows:

$$y^* = \frac{1}{K + ab^{-t}} \quad (5)$$

Wang et al. (2007) compares the trend line as calculated by this curve with the results of the actual field measurement, leaving other theories uncombined. The fitted curve of the measured results is in good agreement with that of the Pearl curve.

The Pearl curve model can reflect the tunneling time–space process. Assuming that $t \to +\infty$ and $y^* \to 1$, $K = 1$ can be obtained. y^* can be used as a factor that reflects the variation of the surface settlement maximum over time above the tunnel. $y^* \cdot S_{max}$ is used to reflect the temporal and spatial variation of the maximum point of settlement in the lateral settling trough in the vertical direction. Equation 6 presents the settlement of point (0, 0, 0) at time t, assuming that the soil below the survey line is excavated at t = 0:
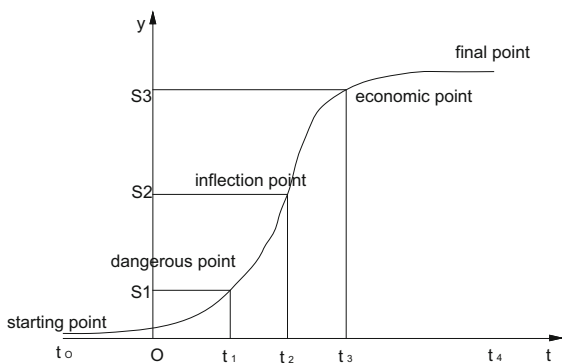
$$S_{(t)} = \frac{S_{max}}{1 + ab^{-t}} \quad (6)$$

where $S_{(t)}$ is the maximum settlement at time t when $t \to +\infty$, $S_{(t)} = S_{max}$, where a is the influence coefficient of early settlement, and b is the coefficient of excavation speed.

3.2 Spatio-Temporal Prediction Model for Surface Settlement of Single-Track Tunnels Under Continuous Construction

Referring to Shi's (2007) hypothesis method on surface settlement, we assume that the layer that predicts surface settlement is homogeneous. When the construction excavation is continuous (the time used for the construction cycle is equal), the tunnel excavation start time is t = 0, and the tunnel is excavated forward at the same speed v (m/day). After time t, the excavation distance D = vt. When the point coordinate D > y, the time that the cross section of the tunnel face passes through the point is $\frac{D-y}{v}$. The settlement value of point (x = 0, y, z = 0) at time t is as follows:

$$S_{(x=0,y,z=0,t)} = S_{max(y,t)} = \frac{S_{max}}{1 + ab^{-\frac{D-y}{v}}} \quad (7)$$

When the cross section of the tunnel face has yet to reach point (x = 0, y, z = 0), $\frac{D-y}{v}$ takes a negative value, and the formula remains correct. We assume that the volume of the settlement trough that is formed by tunnel excavation in the soil layer is equal to the soil loss volume. The settling trough of the same depth stratum retains the same regularity as the surface settling trough. Through regression analysis, the formula that can be drawn is as follows:

$$\frac{S_{max(z)}}{S_{max(0)}} = \frac{i}{i_{(z)}} \quad (8)$$

$$i_{(z)} = i\left(1 - \frac{z}{h}\right)^n \quad (9)$$

This formula is then taken into the Peck formula to obtain point (x, y, z) settlement at time t.

$$S_{(x,y,z,t)} = \frac{S_{max}}{1 + ab^{-\left(\frac{D-y}{v}\right)}} \cdot \frac{1}{\left(1 - \frac{z}{h}\right)^n} \cdot exp\left(-\frac{x^2}{2i^2\left(1 - \frac{z}{h}\right)^{2n}}\right) \quad (10)$$

where $S_{max,f} = \frac{\pi R^2 \eta}{i\sqrt{2\pi}}$.

Fig. 2 Pearl curve model

3.3 Spatio-Temporal Prediction Model for Surface Settlement of Double-Track Tunnels Under Continuous Construction

The double-line tunnel is a common form of tunnel in urban underground rail transit. The left and right tunnels were excavated in sequence, and the settlement troughs caused by the two excavations were superimposed on each other to form a new settlement trough. In a large number of field measurements, the shape of the settlement trough of the double-track tunnel is asymmetrical (Gang 2013; Zheng et al. 2016). Figure 3 illustrates its shape. The peak position of the settlement trough is frequently located above the preceding or rear tunnel due to the influence of construction disturbance and support. Therefore, predicting the settlement cannot use simple superposition calculations. The parameters of the preceding and trailing tunnels should be considered separately.

Mark proposed that the settlement trough caused by the preceding tunnel and additional settlement tank caused by the subsequent tunnel are superimposed to obtain the final settlement tank (Keshuan 2008). The main concept is that the preceding and subsequent tunnels are calculated separately. The i- and η-values of each tunnel are independent and finally superimposed. The final formula is as follows:

$$S_{(x)} = S_{max,f} \cdot exp\left[\frac{-(x - 0.5L)^2}{2i_f^2}\right] + S_{max,s}$$
$$\cdot \, exp\left[\frac{-(x + 0.5L)^2}{2i_s^2}\right] \qquad (11)$$

where $S_{max,f}$ and $S_{max,s}$ are the maximum settlement values; $S_{max,f} = \frac{\pi R^2 \eta_f}{i_f \sqrt{2\pi}}$; $S_{max,s} = \frac{\pi R^2 \eta_s}{i_s \sqrt{2\pi}}$; $\eta = \frac{V_{loss}}{\pi R^2}$; η_f and η_s are the soil loss rate; i_f and i_s are the width coefficients of the settling trough; The subscript f represents the parameters of the tunnel to be
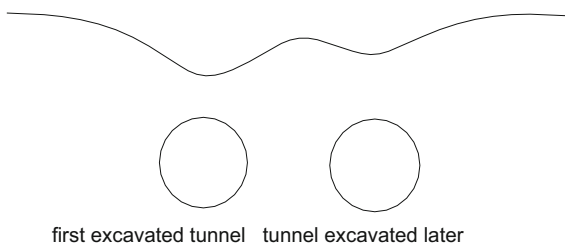
excavated first and the subscript s represents the parameters of the tunnel to be excavated later.

In the prior equations, the intersection of the middle and surface lines of the two parallel tunnels is taken as the coordinate origin O. Taking the excavation of the right tunnel line as an example, L is the space between the two tunnels. Figure 4 displays the top view of the construction.

Considering the parameters of the preceding and trailing tunnels separately reflects the influence of the preceding tunnel on the trailing tunnel. However, doing so can estimate the final settlement only. Taking time t into consideration, only the one-dimensional surface settlement curve is considered. The settlement at time t is as follows:

$$S_{(x,t)} = \frac{S_{max,f}}{1 + ab^{-t}} \cdot exp\left[\frac{-(x - 0.5L)^2}{2i_f^2}\right] + \frac{S_{max,s}}{1 + ab^{-t}}$$
$$\cdot \, exp\left[\frac{-(x + 0.5L)^2}{2i_s^2}\right]$$
$$(12)$$

Assume that the starting time of the first tunnel excavation is t = 0, and the starting time interval of excavation between the preceding and trailing tunnels is t_s Both tunnels are excavated at equal speed v (m/day). After time t, the distance of the first tunnel excavation is $D_f = v_t$, and that of the backward tunnel excavation is $D_s = v(t - t_s)$. The time of passing through point (x, y, 0) of the face of the two tunnels is $\frac{D_f - y}{V}$ and $\frac{D_f - y}{V} + t_s$. When the two tunnels are excavated at the same speed, the settlement value at time t (x, y, 0) is as follows:

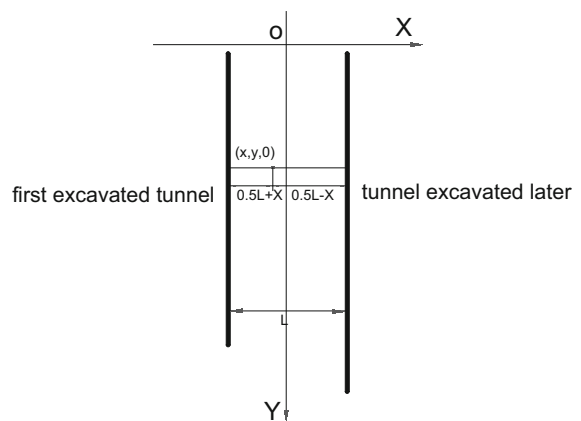Fig. 3 The settlement trough of the double-track tunnel

Fig. 4 Top view of the parallel tunnel

$$S_{(x,y,0,t)} = \frac{S_{max,f}}{1 + ab^{-\frac{D_f - y}{v}}} \cdot exp\left[\frac{-(x - 0.5L)^2}{2i_f^2}\right]$$
$$+ \frac{S_{max,s}}{1 + ab^{-\left(\frac{D_s - y}{v} + t_s\right)}} \cdot exp\left[\frac{-(x + 0.5L)^2}{2i_s^2}\right] \quad (13)$$

According to the derivation method of Eq. (10), Eqs. (8) and (9) are brought into Eq. (13). The three-dimensional space–time prediction formula of stratum settlement of parallel tunnel is as follows:

$$S_{(x,y,z,t)} = \frac{S_{max,f}}{1 + ab^{-\left(\frac{D_f - y}{v_f}\right)}} \cdot exp\left[\frac{-(x - 0.5L)^2}{2i_f^2\left(1 - \frac{z}{h}\right)^{2n}}\right]$$
$$\cdot \frac{1}{\left(1 - \frac{z}{h}\right)^n} + \frac{S_{max,s}}{1 + ab^{-\left(\frac{D_s - y}{v_s} + t_s\right)}}$$
$$\cdot exp\left[\frac{-(x + 0.5L)^2}{2i_s^2\left(1 - \frac{z}{h}\right)^{2n}}\right] \cdot \frac{1}{\left(1 - \frac{z}{h}\right)^n} \quad (14)$$

where $S_{max,f} = \frac{\pi R^2 \eta_f}{i_f \sqrt{2\pi}}$, $S_{max,s} = \frac{\pi R^2 \eta_s}{i_s \sqrt{2\pi}}$, i_f and i_s are the width coefficients of the settling tanks and η_f and η_s are the soil loss rates of the preceding and trailing tunnels, respectively; and $\eta = \frac{V_{loss}}{\pi R^2}$ and L is the distance between the two parallel tunnels.

Non-parallel two-line tunnels are frequently found in underground rail transit, as shown in Fig. 5. In non-parallel tunnels, the previous formula no longer applies. When digging in homogeneous soil, the diffusion in the x and y directions is equal, and the surface settlement trough is circular. The length of the vertical line from point (x, y, 0) to the leading tunnel axis is Lf, and the length of the vertical line from the point to the axis of the trailing tunnel is Ls. In the case

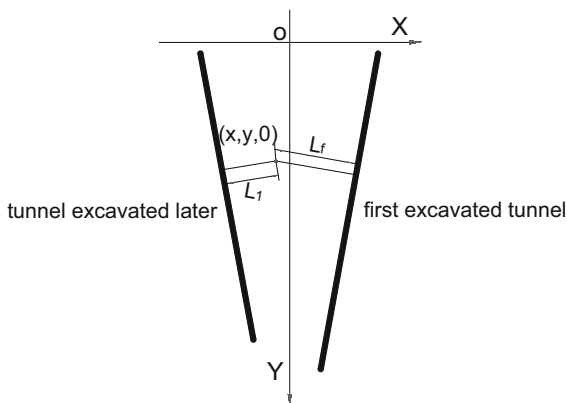where the angle between the two tunnels is small, Eq. (14) can be modified into a three-dimensional space–time prediction formula for formation subsidence, which is suitable for parallel and non-parallel two-line tunnels.

$$S_{(x,y,z,t)} = \frac{S_{max,f}}{1 + ab^{-\left(\frac{D_f - y}{v_f}\right)}} \cdot exp\left[\frac{-(L_f)^2}{2i_f^2\left(1 - \frac{z}{h}\right)^{2n}}\right]$$
$$\cdot \frac{1}{\left(1 - \frac{z}{h}\right)^n} + \frac{S_{max,s}}{1 + ab^{-\left(\frac{D_s - y}{v_s} + t_s\right)}}$$
$$\cdot exp\left[\frac{-(L_s)^2}{2i_s^2\left(1 - \frac{z}{h}\right)^{2n}}\right] \cdot \frac{1}{\left(1 - \frac{z}{h}\right)^n} \quad (15)$$

3.4 Spatio-Temporal Prediction Model for Surface Settlement of Double-Track Tunnels Under Discontinuous Construction

During construction, pauses occur frequently. Thus, the difference in construction speed between the two tunnels should also be considered. When the excavation speed of the two tunnels and dwell time differ, the excavation speed of the first tunnel is expressed as v_f (m/day), and the excavation speed of the subsequent tunnel is v_s. The total time for the first tunnel pause between (0, t) is t_f', and the total time for the subsequent tunnel pause is t_s'. The interval between the start times of excavation of the trailing and preceding tunnels is t_s, such that $D_f = v_f(t - t_f')$ and $D_s = v_s t - t_s' - t_s$. The two-dimensional spatio-temporal prediction formula for soil settlement of a double-track tunnel considering different tunnel excavation speeds and construction pause is as follows:

$$S_{(x,y,0,t)} = \frac{S_{max,f}}{1 + ab^{-\left(\frac{D_f - y}{v_f} - t_f'\right)}} \cdot exp\left[\frac{-(L_f)^2}{2i_f^2}\right]$$
$$+ \frac{S_{max,s}}{1 + ab^{-\left(\frac{D_s - y}{v_s} + t_s - t_s'\right)}} \cdot exp\left[\frac{-(L_s)^2}{2i_s^2}\right] \quad (16)$$

Equations (8) and (9) are substituted into Eq. (16) to obtain a three-dimensional space–time prediction formula for the settlement of a double-line tunnel.

Fig. 5 Top view of non-parallel tunnel

$$S_{(x,y,z,t)} = \frac{S_{max,f}}{1 + ab^{-\left(\frac{D_f - y}{v_f} - t_f'\right)}} \cdot exp\left[\frac{-(L_f)^2}{2i_f^2\left(1 - \frac{z}{h}\right)^{2n}}\right]$$
$$\cdot \frac{1}{\left(1 - \frac{z}{h}\right)^n} + \frac{S_{max,s}}{1 + ab^{-\left(\frac{D_s - y}{v_s} + t_s - t_s'\right)}}$$
$$\cdot exp\left[\frac{-(L_s)^2}{2i_s^2\left(1 - \frac{z}{h}\right)^{2n}}\right] \cdot \frac{1}{\left(1 - \frac{z}{h}\right)^n}$$

$$(17)$$

4 Reliability Analysis of the Modified Peck Formula

4.1 Project Overview

Shenzhen Metro Line 7 starts from Xilihu Station in Nanshan District and ends at Taian Station in Luohu District. It has a total length of 30.173 km and covers 28 underground stations and 27 sections of civil works. The Shenzhen Metro Line 7 Antoshan parking lot entrance and exit line is located in Nanshan District, Shenzhen, north of the Antoshan high slope, at the south side of the construction of a village protection housing. Two-line tunnel segments with mileages of ZKD1 + 117.6–ZKD1 + 161.5 and YDK0 + 716–YDK0 + 665.5 were selected for the research. The right tunnel of the lower crossing section is curvilinear, whereas the left tunnel is linear. The tunnel spacing is 1.2D–3.9D, where D is the width of the cross section of the tunnel at 6.52 m. Figure 6 provides the plan of the project. The tunnel section is horseshoe-shaped and constructed using the bench cut method. The stratigraphic distribution is shown in Fig. 7.
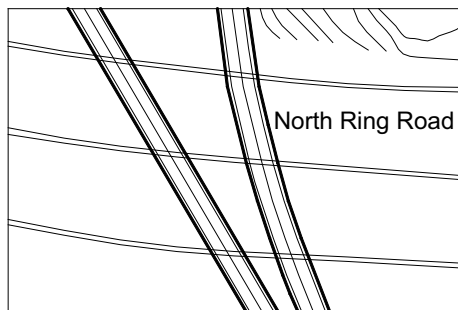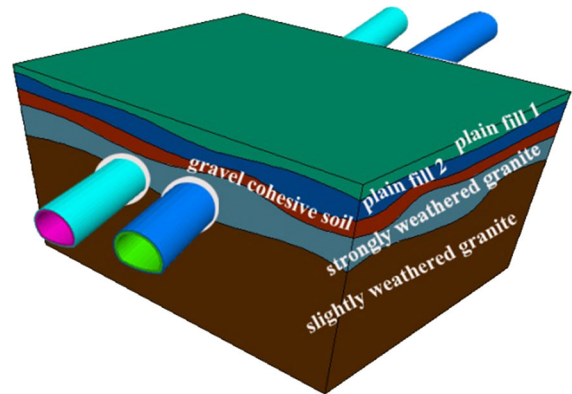

Fig. 6 Project plan

Fig. 7 Stratigraphic distribution

The tunnel is designed and constructed according to the anchor and shotcrete construction method, and the composite lining structure is adopted. The primary support consists of C25 concrete, 200 × 200 mm steel mesh, 0.8 × 0.6 m hollow bolt, and 0.6 m I18 steel frame. The ground is divided into four layers from top to bottom, namely, plain fill, gravel cohesive soil, strongly weathered granite, and slightly weathered granite. Groundwater is mainly pore and feature water in bedrock. Feature water in bedrock mainly exists in strongly and slightly weathered granite, whereas pore water mainly exists in the upper soil layer.

4.2 Numerical Calculation Method

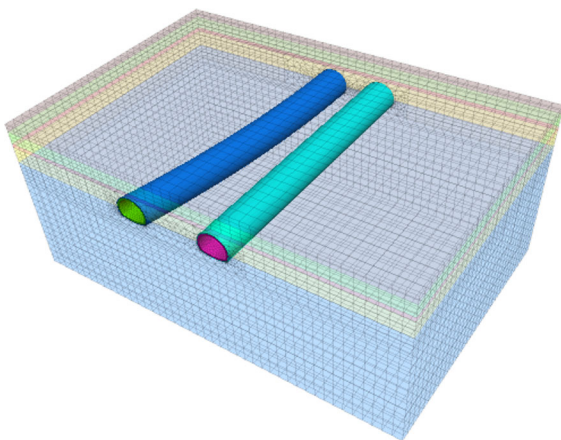#### 4.2.1 Numerical Simulation Model

According to engineering geology and construction drawings and combined with the actual construction conditions, Flac 3D is used to establish a three-dimensional numerical calculation model. The model has a length of 90 m, a width of 60 m, and a height of 40 m. To ensure calculation speed and accuracy, we simplified the modeling of the strata. The tunnel on the left side is excavated in a straight line, whereas the tunnel on the right side is an arc with a radius of 250 m. The cross-sections of both tunnels are horseshoe-shaped with a width of 6520 mm and a height of 6883 mm. The distance between the left and right edges of the tunnel model is approximately 3.0 D, where D is the diameter of the tunnel. The grid is divided by mixed cells, in which the number of units and nodes is 66,589 and 53,067, respectively. The

Mohr–Coulomb model was used for stratigraphic calculations, and the impact of groundwater was disregarded. Figure 8 presents the numerical simulation model.

4.2.2 Parameters and Simulation Process

A large part of the tunnel is located in strongly and slightly weathered granite. The excavation steps of the model are as follows: After calculating the initial self-weight balance, the displacement and speed are zeroed. For the area to be excavated, full-section grouting is taken for leading consolidation. When tunnel excavation is carried out, the lower bench is excavated after the upper bench. The left and right tunnels are divided into 16 steps for excavation. The left-line tunnel starts at excavation depths for the upper and lower benches reach 16 and 12 m, respectively. After each step of the excavation calculation is completed, the initial support calculation is performed.

Mohr–Coulomb model is a general calculation model of geotechnical mechanics, witch can simulate loose or cemented granular materials. According to the manual of engineering mechanics and field test, the parameters of the model are obtained. The related mechanical parameters are shown in Table 1.

Fig. 8 Numerical simulation model

4.3 Reliability Analysis

#### 4.3.1 Monitoring Measurement and Parameter Analysis

Soil settlement is monitored to verify the correctness of the modified Peck formula. In the monitoring and measurement of the construction, three rows of monitoring points are arranged on the road surface, and the distance between the monitoring points in the same row is set to 2 m. Figure 9 shows the location of the monitoring point. In Fig. 9, the red dot represents the location of the detected surface point, and the group (such as group A) represents the position of the multi-point extensometer, which can detect stress and displacement

Figure 10 shows the settlement curve of the right tunnel after excavation over a certain period of time. The point with the largest settlement value is D1 + 161 − 4 above the right vault, and the maximum settlement amount is 25.1 mm. The Gaussian curve was fitted to the data, and the bending points were set to x = 19.2 and x = 32.7. Figure 11 shows the final result and fitting curve. The final settlement of the D1 + 161 line is 29.0 mm, which is less than the settlement control standard at 30 mm. The monitoring points are located inside the settling trough due to the limited conditions onsite. The final settlement curve is subtracted from the preceding tunnel excavation curve to obtain the settlement curve caused by the excavation of the left tunnel, as shown in Fig. 12. After the Gaussian curve fitting, the measured and fitting values of the post-excavation tunnel remain relatively close. The maximum settlement value caused by the excavation of the left tunnel is D0 + 720 − 9 above the left tunnel, and the maximum settlement value is 15.5 mm, which is smaller than the surface settlement caused by the excavation of the right tunnel. The bending points of the settling trough on the left is x = 17.4 and x = 5.0
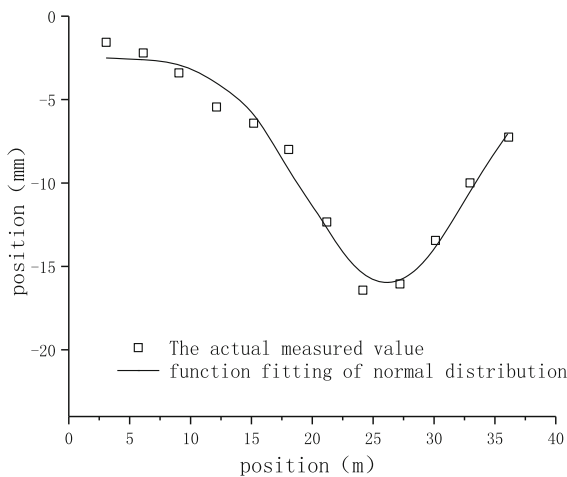
On the basis of Fig. 10, we conclude that $i_f = (32.7 − 19.2)/2 = 6.8$, $i_s = (17.4 − 5.0)/2 = 5.8$. The width coefficient of the settling trough is related to tunnel radius R and buried depth h. The cross-section of the tunnel is approximately circular, whereas the opposite is true for the shape of the tunnel. R = 3.26, we can get the following formula.
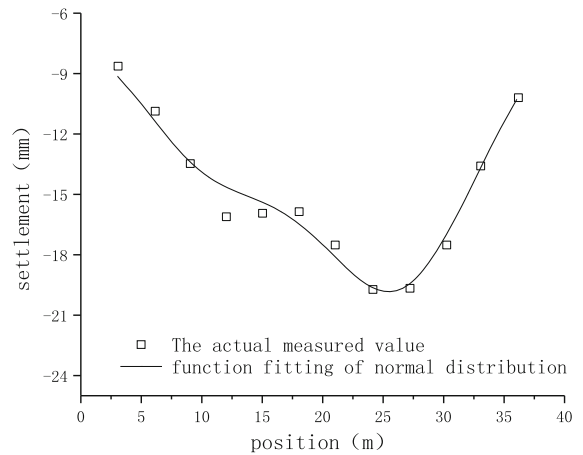
Table 1 Mechanical parameters of different structures

Structure	Elastic modulus (MPa)	Poisson ratio/v	Natural unit weight (kN/m³)	Cohesion (kPa)	Friction angle (°)	Thick (m)
Plain fill 1	8.51	0.35	17.1	10	10	2
Plain fill 2	8.65	0.34	17.6	10	12	3
Gravel cohesive soil	10.20	0.34	17.5	10	12	1.4
Strongly weathered granite	14.10	0.30	19.2	30	34	4
Slightly weathered granite	23.30	0.26	26.8	60	51	26
The upper part of the grouting circle	28.20	0.3	27.0	50	51	–
The lower part of the grouting circle	46.10	0.3	27.0	65	64	–
Primary support	3.43e4	0.2	–	–	–	0.25
Second support	3.43e4	0.2				0.40
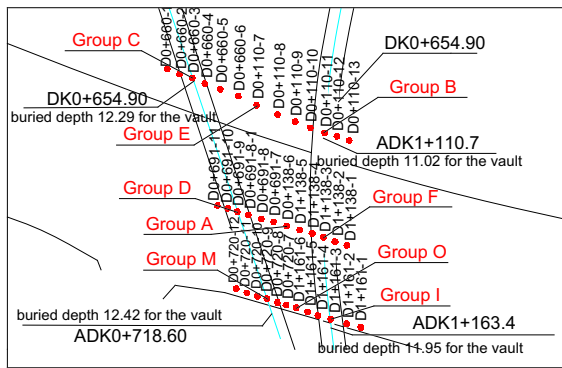
Fig. 9 Arrangement of monitoring points for surface settlement

Fig. 11 Surface settlement curve of two tunnels completed

$$V_{loss,f} = S_{max,f} \cdot i_f \sqrt{2\pi} = 16.3 \cdot 6.8 \cdot \sqrt{2\pi}$$
$$= 277.83 \times 10^3 \text{ mm}^2 \quad (18)$$

$$V_{loss,s} = S_{max,s} \cdot i_s \sqrt{2\pi} = 10.6 \cdot 5.8 \cdot \sqrt{2\pi}$$
$$= 154.1 \times 10^3 \text{ mm}^2 \quad (19)$$

$$\eta_f = \frac{V_{loss,f}}{\pi R^2} = 0.832\% \quad (20)$$

$$\eta_s = \frac{V_{loss,s}}{\pi R^2} = 0.461\% \quad (21)$$

In the back analysis of the values of a and b, single-line or long-distance two-lane tunnels should be selected for analysis to reduce the impact of adjacent tunnel construction. The settlement data of the other

Fig. 10 Surface settlement curve after tunnel excavation on the right side
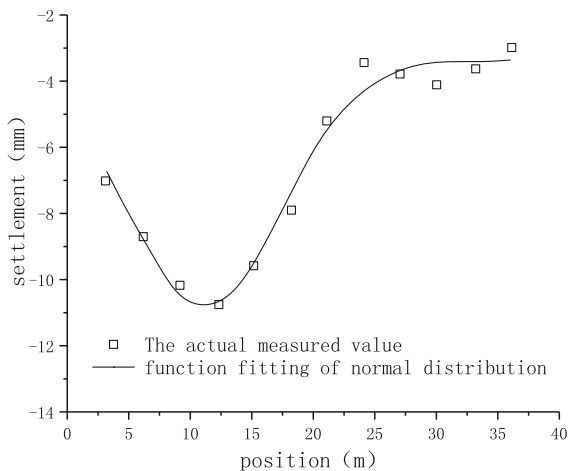
Fig. 12 Surface settlement curve after tunnel excavation on the left side

three monitoring points of the project are analyzed, as shown in Table 2. The settlement value is converted into a positive one during data analysis. Assuming that the tunnel is excavated to the cross-section of the monitoring site, then t = 0. The initial settlement value is S1, whereas the final settlement value is Smax. At t = 0, the following formula should be used:

$$\frac{1}{1 + ab^{-t}} = \frac{S_1}{S_{max}} \tag{22}$$

The values of a in the three groups of data are 6.95, 6.14, and 7.33. The average value a = 6.18 is taken as the value of a in the calculation, and coordinate conversion is performed to determine the t2 value. The value of b is mainly affected by the construction speed, thus, v = 0.8 m/d. $t_2 = 9$ was determined from the monitoring data. On the basis of the formula $t_2 = \frac{\ln a}{\ln b}$, b = 1.22. The buried depth h of the tunnel is 15.8 m. The multi-point displacement data in this project were used to elicit the value of n due to the small number of samples of surface displacement in this area. In

practical applications, the data of other projects that have been excavated or are similar in the region should be used for analysis. In this construction, a total of nine sets of multi-point extensometers were set up to monitor the displacement of the soil. Surface displacement monitoring values were obtained at displacements of 2, 4, 6, and 8 m. Then, the formula $\frac{S_{max(z)}}{S_{max(0)}} = \left(1 - \frac{z}{h}\right)^n$ was used to elicit the value of n. The calculation results are shown in Table 3.

The operational error of the personnel and influence of external disturbances are considered, and the area takes n = − 0.3.

4.3.2 Prediction of Surface Settlement

The derived parameters are brought into settlement Eq. (17) to predict surface settlement and settlement values of deep formations. The values of theoretical derivation are compared with the results of field data and numerical simulations to test the rationality of the formula. The speed of the two tunnels is recognized as identical, that is, v = 0.8 m/d. When the section of the tunnel that is excavated passes through the second row of monitoring points for the first time, the date February 28 and t = 0 are logged. The latter excavation section of the tunnel completely passes through the third row of monitoring points, which is logged at March 29, t = 29. The total time for the excavated tunnel's first pause is $t'_f = 11$, and the total time for the tunnel excavated later pause is $t'_s = 0$. The time interval between the first and second excavated tunnels is $t_s = 13$. $D_f = v_f(t - t'_f) = 10.8$ m, $D_s = v_s(t - t'_s - t_s) = 9.6$ m. The value of $\frac{D_s - y}{V_s}$ in the formula can be measured through on-site construction conditions, which are 18 and 16. Figure 13 provides the predicted, measured, and numerical simulation values of the surface settlement of the second monitoring point at t = 29.

Table 2 Values of monitoring points

Monitoring points	S_1	S_{max}	S_1/S_{max}	a
Group A	1.9	15.11	0.126	6.95
Group B	3.66	26.15	0.140	6.14
Group C	3.29	27.40	0.120	7.33
Average value	–	–	0.129	6.81

Table 3 Calculation table of the value of n

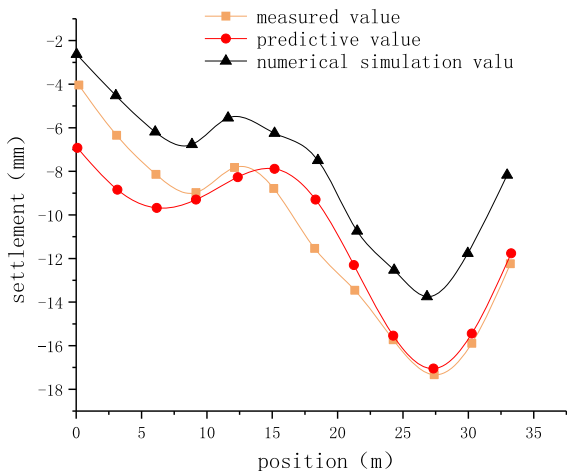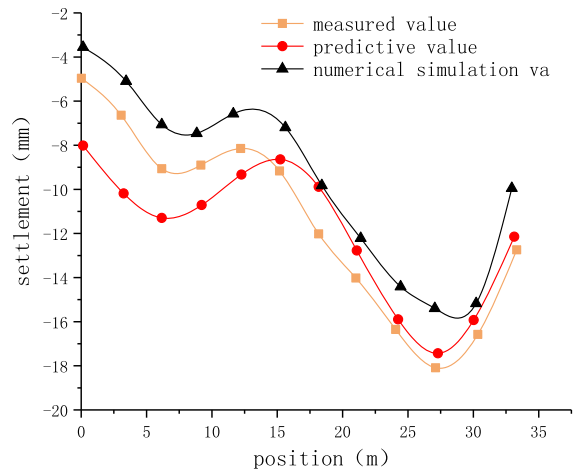| Depth (m)	$\left(1 - \frac{z}{h}\right)$	$\frac{S_{max(z)}}{S_{max(0)}}$	n
2	0.873	1.031	-0.227
4	0.747	1.095	-0.311
6	0.620	1.160	-0.311
8	0.493	1.191	-0.247
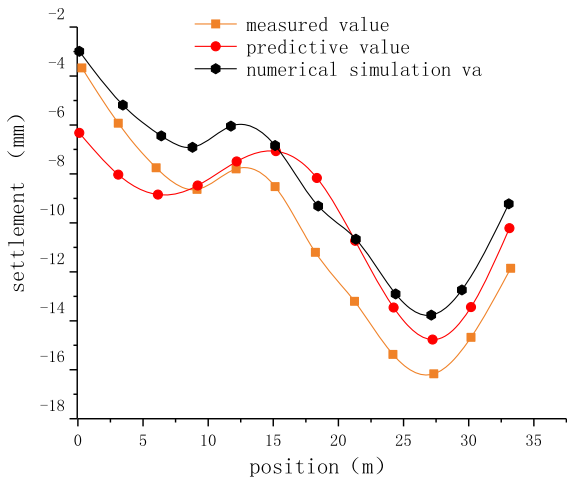
Fig. 13 Comparison curve of surface settlement

The settlement value of the second row on April 10 was obtained using the same method at t = 39 and values of $\frac{D_s - y}{V_s}$ at 28 and 20 after considering the construction pause. Figure 14 displays the comparison of surface settlement at t = 39.

If t is sufficiently large, then the final surface settlement of the second row is obtained. Figure 15 illustrates the comparison of surface settlement.

Considering the measurement error and influence of grouting, the prediction results of the three groups in varying times are in good agreement with the measured and numerical simulation values. We see that the numerical simulation value is the smallest, and the trend is the same as those for the measured and predicted values. The predicted value of the first

Fig. 14 Comparison curve of surface settlement

excavated tunnel is less than the measured value. At t = 29, the settlement prediction value of the first excavated tunnel differs from the monitored value by 2.2 mm. At t = 39, the maximum difference between the predicted value of the settlement of the first excavated tunnel and measured value is 2.5 mm. The settlement prediction value of the second excavated tunnel is larger than that of the measured value, with numerical simulation value as the smallest. This phenomenon is mainly due to the fact that during the derivation of ground loss, the measured value of the double-line tunnel is used to derive the parameters. The accumulation date of the settlement value of the first excavated tunnel is short, and the soil above the tunnel has undergone consolidation settlement. In addition, the formation is assumed to be homogeneous in the calculation process of the surface settlement formula. However, in the actual process and numerical simulation, a heterogeneous formation is adopted. In general, the difference between the predicted and measured values is small, the shape of the settling trough is consistent, and the formula has a high reference value.

4.3.3 Settlement Prediction of Soil Under the Surface

The settlement of soil at depths of z = 2, 4, 6, and 8 m below the multi-point extensometer (point D) was analyzed. The existing parameters are substituted into Eq. (17). In the case of considering the change in z, Eqs. (2)–(17) becomes the following formula.

Fig. 15 Contrast curve of final surface settlement

$$S_{(x,y,z,t)} = \frac{S_{max,f}}{1 + ab^{-\left(\frac{D_f - y}{v_f} - t'_f\right)}} \cdot exp\left[\frac{-(L_f)^2}{2i_f^2\left(1 - \frac{z}{\hbar}\right)^{2n}}\right] \cdot \frac{1}{\left(1 - \frac{z}{\hbar}\right)^n}$$

$$+ \frac{S_{max,s}}{1 + ab^{-\left(\frac{D_s - y}{v_s} + t_s - t'_s\right)}} \cdot exp\left[\frac{-(L_s)^2}{2i_s^2\left(1 - \frac{z}{\hbar}\right)^{2n}}\right] \cdot \frac{1}{\left(1 - \frac{z}{\hbar}\right)^n}$$

$$= \frac{S_{max,f}}{1 + 6.18 \cdot 1.22^{-\left(\frac{D_f - y}{v_f} - t'_f\right)}} \cdot exp\left[\frac{-(L_f)^2}{2 \cdot 4.5^2\left(1 - \frac{z}{15.8}\right)^{2\times 0.3}}\right]$$

$$\cdot \frac{1}{\left(1 - \frac{z}{15.8}\right)^{0.3}} + \frac{S_{max,s}}{1 + 6.18 \cdot 1.22^{-\left(\frac{D_s - y}{v_s} + t_s - t'_s\right)}}$$

$$\cdot exp\left[\frac{-(L_s)^2}{2 \cdot 4.2^2\left(1 - \frac{z}{15.8}\right)^{2\times 0.3}}\right] \cdot \frac{1}{\left(1 - \frac{z}{15.8}\right)^{0.3}}$$

$$\tag{23}$$

A multi-point extensometer was buried at point D0 + 691 − 9, and a multi-point displacement curve was measured in the field, as shown in Fig. 16. Certain monitoring data are inaccurate due to the large number of interference sources at the construction site. However, the data in the figure maintain an obvious regularity. The displacement data in the figure show that the relative displacement of the formation increases with the increase in depth. The displacement of the formation recorded by the multi-point extensometer at a depth of 8 m reached 1.9 mm.

On the basis of Formula 23, the prediction results of the deep soil settlement at the D0 + 691 − 9 points are obtained and compared with the field test results, as shown in Table 4.
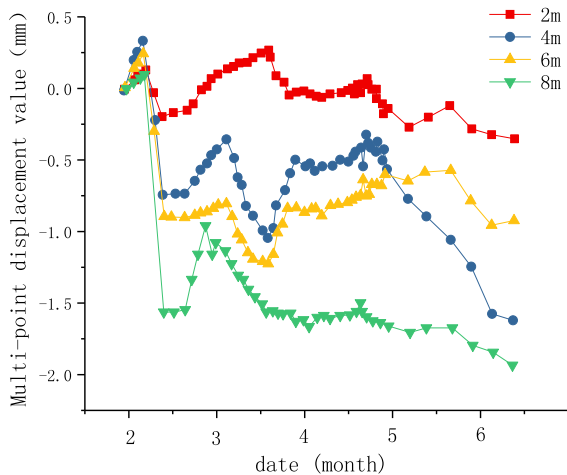
Table 4 Deep soil displacement below point D

Depth (m)	Predicted value of settlement	Relative surface prediction	Actual measured value of relative displacement
2	9.21	0.19	0.08
4	9.46	0.44	0.49
6	9.79	0.77	0.79
8	10.27	1.24	1.57

A comparison of the data in the table indicates that the other results are largely similar except at a depth of 2 m. The settlement at this depth is significantly affected by ground construction, and an error occurs during personnel measurement. Thus, the monitoring results are in good agreement with the predicted results, with the exception of the 2 m point.

We analyzed ground settlement at a depth of 4 m. Figures 17 and 18 provide the results of the theoretical derivation and numerical simulation.

The figures show that the settlement of the tunnel stratum is saddle-shaped, and the predicted value of ground subsidence theory is approximately the same as the numerical simulation at a depth of 4 m. At this depth, the predicted value of ground settlement is roughly similar to the trend of the numerical simulation results. The theoretical prediction value is approximately 5% larger than that of the numerical simulation. The prediction of ground settlement is reliable when time factors are considered.

5 Conclusion

In summary, this paper considers the Shenzhen Metro Line 7 parking lot access line project and proposes a three-dimensional space–time prediction calculation formula for double-line tunnel surface settlement. The results of the study are as follows:

1. Relying on the Shenzhen Metro Line 7 parking lot access line project, numerical simulation, actual monitoring, and theoretical derivation were used to study the law of surface settlement. The prediction model of surface settlement of tunnel construction based on the Pearl curve model is proposed, and the calculation formula of surface settlement under different construction conditions is derived. A comparison among the modified

Fig. 16 Field measured multi-point displacement curve at point D0 + 691 − 9
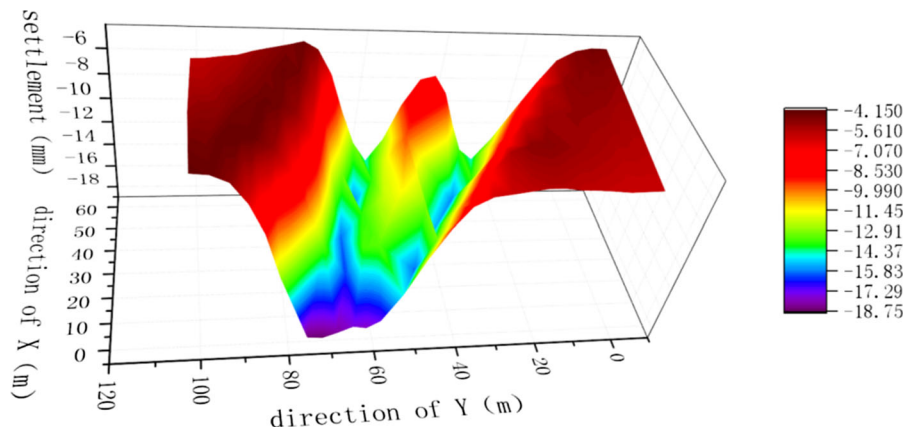
Fig. 17 Theoretically derived prediction of formation subsidence

Fig. 18 Numerical simulation value of formation subsidence
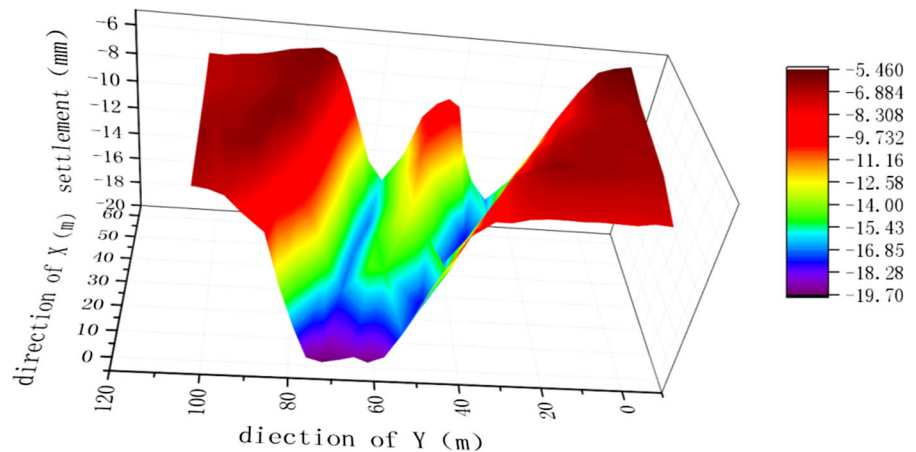
Peck formula, numerical simulation, and actual measurement shows that the results of the three-dimensional space–time prediction of the surface settlement of the double-line construction tunnel are more reliable.

2. The influence of time factors and depth on the prediction of surface subsidence is considered, and the calculation formula of the three-dimensional space–time prediction for the settlement of two-line tunnels is derived. The derived modified Peck formula is characterized by the following: (1) the influence of time factors on the surface settlement of tunnel excavation is considered. The derived formula of surface subsidence can calculate the surface subsidence at varying times, and (2) on the basis of the Pearl curve model, the ground settlement prediction model can calculate formation settlement at different depths.

3. The mechanism of ground deformation caused by tunnel excavation and the general law of stratum settlement are elucidated. When the two-lane tunnel is excavated, construction stoppage will increase surface settlement. Thus, ground deformation cannot be simply superimposed, and the influence of the tunnel excavation sequence should be considered.

References

An J (2015) Model test and theoretical calculation of the interaction between shallow tunnel excavation and foundation load of existing buildings. Dissertation, Beijing Jiaotong University

Changming H, Chao F, Yuan M et al (2018) Improvement of Peck settlement prediction formula for shield tunnel construction in Xi'an water-rich sand layer. Chin J Undergr Space Eng 14(01):176–181

Chen C, Zhao C, Wei G et al (2014) Prediction of soil settlement induced by double-line shield tunnel based on Peck formula. Rock Soil Mech 35(08):2212–2218

Gang W (2013) Prediction of soil settlement caused by double-line parallel shield tunnel construction. Disaster Adv 6(6):23–27

Gang W, Yangkan Z (2016) A simplified method for predicting ground settlement caused by adjacent parallel twin shield tunnel construction based on stochastic medium theory. Rock Soil Mech 37(S2):113–119

Kang Z, Gong Q, He C et al (2014) Modified Peck equation method for shield tunnel oblique crossing upper railway. J Tongji Univ Nat Sci 42(10):1562–1566

Ke W, Wen Z, Wu H et al (2016) Study of impact of metro station side-crossing on adjacent existing underground structure. J Intell Fuzzy Syst 31(4):2291–2298

Keshuan M (2008) Research on foundation movement and adjacent building protection caused by shield construction. Dissertation, Huazhong University of Science and Technology

Li X, Li S, Li S et al (2012) Study with geomechanical model test on surface subsidence of extremely shallow large-span double-arch tunnel. J Wuhan Univ Technol (Transm Sci Eng) 36(6):1118–1121

Litwiniszyn J (1956) Application of the equation of stochastic processes to mechanics of loose bodies. Arch Mech 8(4):393–411

Peck RB (1969) Deep excavation and tunneling in soft ground. In: State of the art report, 7th international conference on soil mechanics and foundation engineering, Mexico City, pp 225–290

Shi C (2007) Time-space unified prediction theory and application research of urban tunnel construction stratum deformation. Dissertation, Central South University

Wang X, Wang Y, Yu F (2007) Research and application of Peel-adaptive immune algorithm in intelligent calculation of tunnel surrounding rock. Chin J Rock Mech Eng 26(a01):3410–3415

Yandong Y, Kui C, Fengyuan L et al (2014) Study on horizontal ground settlement of shield tunneling in the land section of lion ocean tunnel. Tunnel Constr 12:1143–1147

Zhang W, Ke WU, Haotian WU et al (2016) Assessing the influence of humidity on the stability of expansive soil rock surrounding tunnels. Int J Simul Syst Sci Technol 17(44):291–295

Zheng Y, Ji J, Yuan Z et al (2016) Study on the influence zone and construction control of subway tunnels underpassing existing railways. Mod Tunn Technol 53(6):202–209

Zhu Z, Huang S, Zhu Y (2012) Research on road subsidence law and control standard caused by railway tunnel underpassing highway. Rock Soil Mech 33(2):558–563